Hindawi
Journal of Sensors
Volume 2020, Article ID 3124102, 13 pages
https://doi.org/10.1155/2020/3124102

Research Article

One-Pot Synthesized Nickel-Cobalt Sulfide-Decorated Graphene Quantum Dot Composite for Simultaneous Electrochemical Determination of Antiretroviral Drugs: Lamivudine and Tenofovir Disoproxil Fumarate

Ruvimbo Chihava, Daniel Apath, Mambo Moyo, Munyaradzi Shumba, Vitalis Chitsa, and Piwai Tshuma

Sensor Lab Research Group, Department of Chemical Technology, Midlands State University, Private Bag 9055, Senga, Gweru, Zimbabwe

Correspondence should be addressed to Mambo Moyo; moyom@staff.msu.ac.zw

Received 6 December 2019; Revised 10 February 2020; Accepted 14 February 2020; Published 2 July 2020

Academic Editor: Hana Vaisocherova - Lisalova

In the present study, simultaneous electrochemical behavior of tenofovir disoproxil fumarate (TDF) and lamivudine (LAM) on a glassy carbon electrode (GCE) modified with a novel nanocomposite, nickel-cobalt sulfide-decorated graphene quantum dots (Ni-CoS/GQDs) was investigated. Characterization of different components used for modifications was achieved using UV-Vis and transmission electron microscopy (TEM). The electrochemistry of TDF and LAM at the modified electrode was examined using cyclic voltammetry (CV), linear sweep voltammetry (LSV), chronoamperometry, differential pulse voltammetry (DPV), and electrochemical impedance spectroscopy (EIS). A substantial (+39 mV TDF; +20 mV LAM) decrease in potential on oxidation reaction in 0.1 M PBS (pH 8.0) was achieved due to synergy between Ni-CoS and GQDs. Using optimized voltammetric parameters and pH, DPV gave a linear calibration over the range 5-18 μM for TDF and LAM. The detection limits were calculated as 2.42×10^{-8} mM (LAM) and 1.21×10^{-8} mM (TDF). The estimated values for Gibbs free energy revealed adsorption of TDF and LAM on Ni-CoS/GQDs/GCE as a spontaneous and favorable process. The voltammetric method was applied for determination of LAM and TDF in a pharmaceutical formulation giving average recovery of 99.65%.

1. Introduction

The treatment of infections for human immunodeficiency viruses (HIV) causing immunodeficiency syndrome (AIDS) is accomplished through the use of antiretroviral drugs [1]. Among the group of antiretroviral drugs, tenofovir disoproxil fumarate (TDF) (Figure 1(a)) is a nucleotide reverse transcriptase inhibitor whilst lamivudine (LAM) (Figure 1(b)) is a nucleoside reverse transcriptase inhibitor, both active against HIV-1, HIV-2, and hepatitis B virus [2]. The mode of action is by blocking the HIV reverse transcriptase enzyme through inhibition. The need to improve analytical work involving drugs is significant. A growing demand for drugs throughout the world stimulates a search for new and even more effective drug-monitoring techniques. Therefore, it is pertinent to fabricate new and improve on the existing analytical methods regarding their qualitative and quantitative analysis.

Literature survey has revealed HPLC [3–5], spectrophotometry [6–8], UV-Vis spectroscopy [9–11], and electrochemical [12] as possible methods for the determination of TDF and LAM in different matrices. However, demerits such as time-consuming, expensiveness, and need for qualified technicians have been encountered. Electrochemical techniques have shown perfectness in the determination of drugs in various matrices without any extraction or evaporation

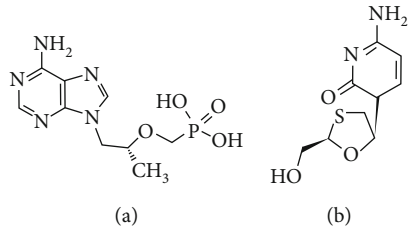

Figure 1: Chemical structure of tenofovir disoproxil fumarate (a) and lamivudine (b).

steps [9, 13]. Extensive literature has shown that most researchers concentrated on electrochemical reduction of TDF at hanging mercury drop electrode [14] for which mercury is not environmentally friendly if not handled with care. Recently, Ozcelikay et al. reported oxidation of TDF at bare glassy carbon electrode [15]. However, determination of drugs on bare glassy electrodes can lead to electrode fouling and higher overpotential [13]. Single determinations of LAM in human serum and plasma have been reported through electrochemical means [16–18]. Overall, it is worthwhile for electrochemists to use voltammetric techniques frequently with different modifiers as options as evidenced by working principles which are easy to follow, instrumentally simple, costly, and portable.

The use of inorganic materials, such as Ni, Co, their corresponding oxides, and sulfides, has attracted interest in sensor development in recent years [19, 20] as a result of low cost, nontoxicity, easy production, high specific surface area, good electrocatalytic activity, and facile electron transfer at lower potential. Specifically, binary transition-metal sulfides, i.e., $NiCo_2S_4$, have recently been considered as promising electrode materials offering richer redox reactions owing to the contributions of both nickel and cobalt with different valence states, narrow band gap, and higher electronic conductivity due to the presence of sulphur [21–23]. However, the nonnoble transition electrocatalysts highlighted (Ni, Co) show stronger aggregation on electrodes as a result of van der Waal forces causing poor oxidation kinetics [20, 21]. Furthermore, the combination of transitional metals with sulfide forms supercapacitors. Hence, in electrochemical applications to reduce ohmic resistance and improve charge transfer on electrodes, decoration of well-dispersed catalysts on an electronically conductive support is desirable.

Graphene quantum dots (GQDs) are a kind of zero-dimensional material with characteristics similar to graphene and carbon dots as shown by their use in fuel cells [24], supercapacitors [25], and sensors [26]. GQDs have been reported to expand contact area with the analyte during electrochemical analysis [27]. As far as we know, little has been paid on the integration of GQDs with transition metal ions for electrochemical sensing of drugs. Herein, we developed an electrochemical sensor based on GQDs as a burgeoning support to disperse semiconductor nanomaterials (Ni-CoS composite) for novel electrocatalytic efficiency. To the best of our knowledge, this is the first report on the simultaneous oxidation of determination of TDF and LAM on graphene quantum dots decorated by nickel-cobalt sulfide. The simultaneous determination has been necessitated by the fact that electrochemical and enzymatic oxidation pathways of drugs follow similar mechanism [15]. We have illustrated that Ni-CoS/GQDs/GCE exhibited a much higher electroactivity than individual GQDs and Ni-CoS for the simultaneous oxidation and detection of TDF and LAM. Notably, a substantial (+39 mV; +20 mV) decrease in potential for TDF and LAM oxidation reactions, respectively, was observed using Ni-CoS/GQDs/GCE compared to GCE.

2. Experimental

2.1. Chemicals and Instrumentation. All chemicals used were of analytical grade and needed no further purification upon use. Potassium ferricyanide ($K_3Fe(CN)_6$) and potassium ferrocyanide ($K_4Fe(CN)_6$) were obtained from Sigma-Aldrich (South Africa); dipotassium hydrogen phosphate (K_2HPO_2), potassium dihydrogen phosphate (KH_2PO_4), dimethyl formamide (DMF), nickel nitrate ($Ni(NO_3)_2{\cdot}6H_2O$), cobalt nitrate ($Co(NO_3)_2{\cdot}6H_2O$), ethylene glycol (EG), absolute ethanol, and thiourea were obtained from Associated Chemical Enterprises (South Africa). Pharmaceutical formulations were purchased from a local pharmacy. Stock solutions of lamivudine (LAM) and tenofovir disoproxil fumarate (TDF) were prepared by dissolving an appropriate amount of the drug in double-distilled deionized water. All other solutions were prepared using ultra-Millipore water from Milli-Q Water Systems (Millipore Corp., Bedford, MA, USA). All experiments were carried out at room temperature.

Transmission electron microscopy (TEM) image was obtained from a Zeiss Libra TEM 120 model operated at 90 kV using carbon-coated 200-mesh grids. The UV-Vis spectra of composites were obtained using UV-visible spectroscopy Lamda-950, Perkin Elmer, Germany. Electrochemical experiments were performed using Autolab Potentiostat PGSTAT302N equipped with NOVA version 1.10 software employing a conventional three-electrode system. A glassy carbon electrode (GC, 3 mm diameter) was used as working electrode. A platinum electrode was applied as the counter electrode and an Ag/AgCl electrode served as reference. For electrochemical impedance spectroscopy (ESI), a frequency of 100 kHz to 0.01 Hz was employed. All solutions were purged with high-purity nitrogen for at least 15 min to remove oxygen prior to the experiments.

2.2. Synthesis GQDs. Graphene quantum dots (GQDs) were synthesized using a graphene oxide (GO) precursor obtained through Hummer's method, as reported in our previous work [28]. Briefly, 480 mg of GO was added in 48 mL of *N-N* dimethyl formamide (DMF) to produce 10 mg/mL suspension for 1 h, transferred into a 60 mL Teflon bottle held in a stainless steel autoclave and heated in the muffle furnace to 100°C for 8 h. The final GQDs/DMF product was obtained through vacuum filtration using 0.22 μm micropore filter membrane. The suspension was rotated for evaporation to remove DMF, and obtained GQDs were then dissolved in different solvents such as pure water and phosphate buffer solution (PBS) to produce different suspensions [29].

2.3. Synthesis of Ni-CoS/GQD Nanocomposite. Briefly, 20 mg of the prepared GQDs was dispersed in 60 mL of ethylene glycol (EG) through ultrasonication to form a homogeneous GQD suspension for 30 min. The required amounts of Ni $(NO_3)_2{\cdot}6H_2O$ and $Co(NO_3)_2{\cdot}6H_2O$ were added into the prepared suspension slowly, followed by stirring the solution at 80°C for 2 h [30, 31]. Consequently, 6 mmol of thiourea was added to the solution and stirring done for 1 h and then refluxed at 180°C for 2 h [21, 32]. After cooling the solution at room temperature, the product was collected by centrifugation, washed with deionized water and absolute ethanol for several times, and then dried in a vacuum oven at 30°C for 8 h. The final product was designated as Ni-CoS/GQDs. For comparison, a pure Ni-CoS precursor was synthesized in the absence of GQDs following same experimental parameters.

2.4. Electrode Preparation. Prior to the modification, the GCE was polished with 1.0, 0.3, and 0.05 μm alumina slurry, respectively, and sonicated in absolute ethanol and double-distilled water and then dried with high-purity nitrogen steam. Ni-CoS/GQDs/GCE was prepared by casting optimized 5 μL of Ni-CoS/GQD suspension (1 mg/mL Ni-CoS/GQDs in ethanol) on GCE surface and dried at room temperature. For comparison, GQDs and Ni-CoS-modified GCEs were prepared in the same way through a drop-dry method.

2.5. Application

2.5.1. Determination of TDF and LAM in Formulation Tablets. TDF and LAM were simultaneously analyzed in a three-component tablet formulation containing efavirenz. Five tablets were weighed and ground in a mortar to obtain the homogeneous fine powder. A portion of the powder equivalent to a stock solution of the required concentration was transferred into a 25 mL calibrated flask and topped up with deionized water. The mixture was sonicated for a reasonable time until dissolution had occurred. Standard solutions were prepared from the stock through dilution. Voltammograms were recorded using DPV parameters as in pure TDF and LAM. The amounts of TDF and LAM per solution were calculated using calibration curve of pure TDF and LAM, respectively.

2.5.2. Determination of TDF and LAM in Urine Samples. The use of Ni-CoS/GQDs/GCE is investigated for the measurement of TDF and LAM in four human urine samples. Urine samples (5 mL) were taken in a series of 25 mL standard flasks after being collected from healthy volunteers not taking the drugs. Same quantities of TDF and LAM were added to the urine samples and then quantitatively diluted using PBS. The electrochemical behavior of the prepared solutions on Ni-CoS/GQDs/GCE was studied by DPV, and the unknown concentrations were determined from the calibration graph.

3. Results and Discussion

3.1. Physical Characterization. Figure 2 shows the UV-vis absorption of synthesized GO and GQDs. Both GO (a) and

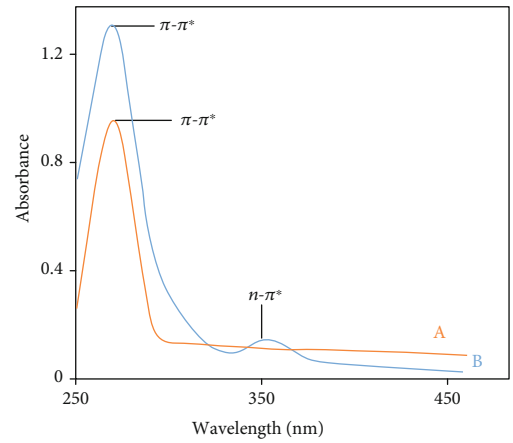

Figure 2: UV-Vis spectra of (a) GO and (b) GQDs.

GQDs (b) dispersions display a maximum absorption peak at 270 nm due to the $\pi - \pi *$ transition of aromatic C=C bonds and an additional absorption peak at 364 nm for GQDs which corresponds to the $n - \pi *$ transition of the C=O bond [33, 34].

The morphology of Ni-CoS nanoparticles and GQDs was investigated using TEM. The Ni-CoS nanoparticles (Figure 3(a)) indicates a random distribution of dark transitional metal nanoparticles with agglomeration. The GQDs show small size and circular shape uniformly dispersed without agglomeration. The particles have a diameter ranging from 1 to 8 nm as shown in the histogram (Figure 3(b)), and it is closed to the zero-dimensional state [35]. The typical wrinkled morphology of GO (inset) from where GQDs were synthesized is exfoliated into single and thin layers [36]. Furthermore, the X-ray diffraction (XRD) patterns of the as-prepared Ni-CoS and Ni-CoS/GQD nanocomposite are shown in Figure 3(c). The other four major peaks at peak 2: 31.5° (311), peak 3: 38.3° (400), peak 4: 50.4° (511), and peak 5: 55.3° (440) can be indexed of the Ni-CoS phase [37]. On comparison of the two XRD images, a weak and broad peak at peak 1: 26.8° (220) appears in the Ni-CoS/GQD nanocomposites, indicating the presence of GQDs.

3.2. EIS and CV Studies. ESI has recently received attention in sensor technology as one of the most powerful tools and non-destructive techniques for monitoring the interfacial electron transfer kinetics at modified electrodes [13]. In this technique, the electron transfer limited process is shown by a semicircle portion at high frequencies whilst a diffusion-limiting step of the electrochemical process is shown by a linear part at lower frequencies. It is noteworthy that the presence of semicircle diameter in the spectra shows the electron transfer resistance (R_{et}). The equivalent circuit model (inset in Figure 4) was used to fit the impedance data into R_{et} values. After each modification stage, the impedance spectra were recorded in 1 M KCl containing 2 mM $[Fe(CN)_6]^{3-/4-}$ as a redox probe (Figure 4). The R_{et} at the bare electrode surface was 900 Ω. A decrease in semicircle diameter is shown after drop casting the Ni-CoS on the GCE, showing the presence of a conductive material on the GCE (R_{et} = 750 Ω). Incorporating the GQDs on the GCE gave

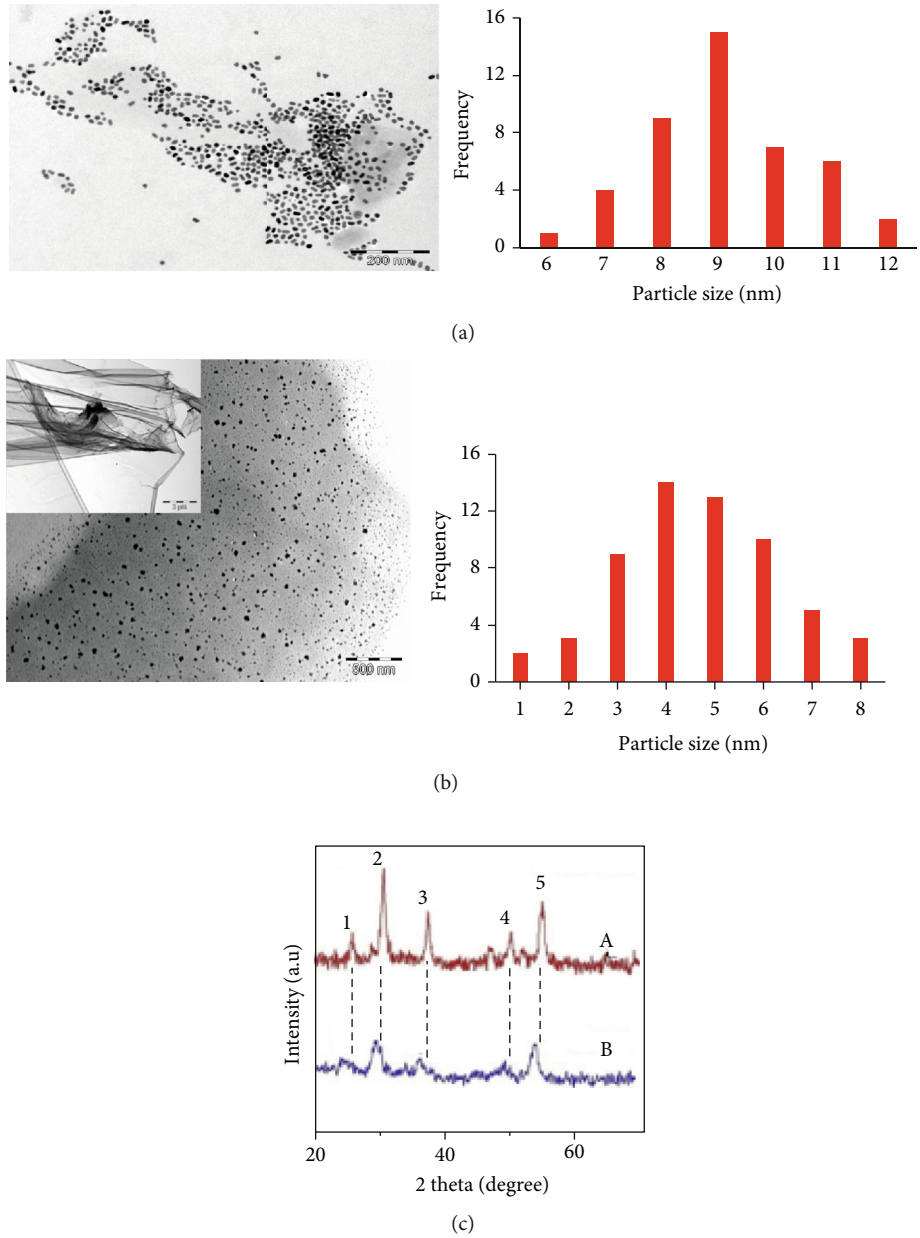

FIGURE 3: (a). TEM of Ni-CoS nanoparticles ×50 nm (b) GQDs ×50 nm: the *inset* shows the surface of GO sheets. (c) XRD patterns of Ni-CoS nanoparticles (A) and Ni-CoS/GQDs (B).

R_{et} = 500 Ω, showing successful modification. By drop casting a combination of Ni-CoS and GQDs, a further decrease in R_{et} (270 Ω) revealing high electrical conductivity increased surface area and favorable electrocatalytic behavior was observed. The order as deduced from impedance values is GCE > Ni-CoS/GCE > GQDs/GCE > Ni-CoS/GQDs/GCE. All changes in R_{et} suggested successful modification of the modified electrode; hence, the electrode based on Ni-CoS/GQD composite was used throughout the study.

By plotting of phase shift vs. log frequency (f), extra information which cannot be obtained from the Nyquist plot is displayed [13]. Figure 4(b) shows Bode phase angle plots in the case of 2 mM $[Fe(CN)_6]^{3-/4-}$ in 1 M KCI with phase angle values for all electrode surfaces less than the ideal 90° for a true capacitor, i.e., phase angle for bare GCE (62°), Ni-CoS/GCE (45°), GQDs/GCE (38°), and Ni-CoS/GQDs/GCE (30°). The information obtained depicts that modified electrodes show catalytic behaviors different from each other since phase angles shifted to different frequencies. Finally, it was concluded that the electron transfer process on the Ni-CoS/GQDs/GCE is possible.

The behavior of modified electrodes was also investigated using cyclic voltammetry at a scan rate of 100 mV/s (Fig S1). Redox peaks were observed on all tested electrodes with different i_p and peak potential separation (ΔE_p). After

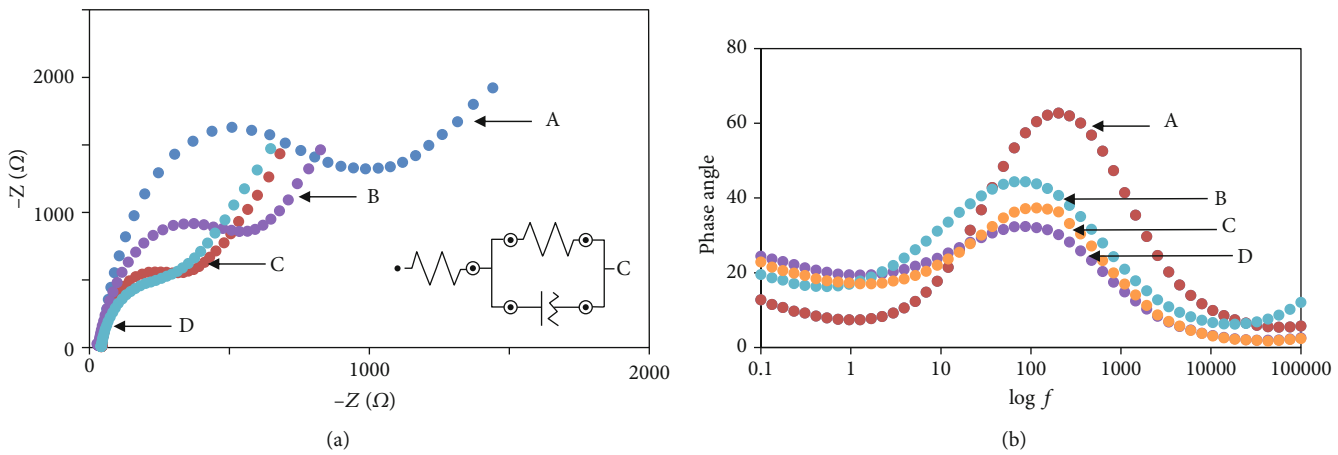

FIGURE 4: (a) Nyquist plots obtained in 2 mM $[Fe(CN)_6]^{3-/4-}$ in 1 M KCI; (b) Bode plots (A) GCE, (B) Ni-CoS/GCE, (C) GQDs/GCE, and (D) Ni-CoS/GQDs/GCE.

immobilization of the Ni-CoS on the surface of GCE, both i_{pa} and i_{pc} increased compared to i_{pa} and i_{pc} of the bare GCE. This phenomenon can be related to the Ni-CoS particles offering a large surface and good conductivity. The GQDs acted as a suitable mediator to shuttle electron hence showed improved peak currents when placed on the GCE. After incorporating the Ni-CoS and GQDs on GCE, a synergistic process could be observed as shown by high i_{pa}, i_{pc}, and reduced E_p. The ΔE_p for a reversible system such as $[Fe(CN)_6]^{3-/4-}$ can be used as a good measure of electron transfer ability of electrodes with lower values depicting a good electron transfer ability [38], with the following trend GCE < Ni-CoS/GCE < GQDs/GCE < Ni-CoS/GQDs/GCE. This confirmed the EIS results.

3.3. pH Studies. One of the main factors influencing height and morphology of an electroactive compound signal is acidity of supporting electrolyte [39]. Hence, the effect of pH during simultaneous oxidation of LAM and TDF on Ni-CoS/GQDs/GCE was investigated by CV in the pH range 4-10 at 100 mV/s (Figure 5). As shown in Figures 5(b) and 5(c), i_{pa} increased from pH 4 to 8 and then decreased to pH 10 for both drugs. It can be observed that E_{pa} values for both drugs shifted to less positive with increasing pH, showing deprotonation in oxidation processes at higher pH. Plots for E_{pa} vs. pH (Figures 5(b) and 5(c)) showed linear relationships for LAM (a slope value of 61 mV/pH) and TDF (a slope value of 46.1 mV/pH). Both values are close to the theoretical value of 59.0 mV/pH [40] indicating that the electron transfer is accompanied by an equal number of protons in electrode reactions.

3.4. Simultaneous Electrochemical Responses of LAM and TDF. CVs of 1 mM LAM and TDF in 0.1 M PBS (pH 8.0) at GCE (A), Ni-CoS/GCE (B), GQDs/GCE (C), and Ni-CoS/GQDs/GCE (D) at a scan rate of 100 mV/s are shown (Figure 6(a)). Electrochemically irreversible characteristics with oxidation peaks on GCE (+203 mV; +637 mV), Ni-CoS/GCE (+208 mV; +618 mV), GQDs/GCE (+225 mV; +618 mV), and Ni-CoS/GQDs/GCE (+223 mV; +598 mV) for LAM and TDF, respectively, were deduced. The source of a current signal is as a result of (in this case) oxidation of each drug. As such, it may be argued that the availability of an avalanche of delocalized electrons and good hole transporting ability in GQDs offer an efficient platform for electron exchange acting as an electron sink [41]. On the other hand, the readily available and accessible d-orbitals in the mixed metal nanoparticles enhance the oxidation ability of the drugs hence efficient electroactivity and detection. However, modifying the electrode with Ni-CoS, GQDs, and Ni-CoS/GQDs/GCE, i_{pa} increases by 1.0, 1.3, and 1.5 times for TDF, respectively, when compared to the value of the unmodified electrode. Electrochemical reaction enhancement of Ni-CoS/GQD composite towards both drugs may be ascribed to three major steps.

Firstly, it is possible that GQDs provide a large amount of anchoring sites for Ni-CoS during composite formation and possibly controlled decoration of nanoparticles without aggregation. Furthermore, the well dispersion of Ni-CoS on the surface of GQDs might have rendered more accessible surfaces for electrocatalysts for possible successful simultaneous oxidation of TDF and LAM. Secondly, the ability of GQDs to expand contact area [27] and its high conductivity might have resulted in fast electron transfer within the composite. Lastly, the presence of small-sized Ni-CoS nanoparticles in the composite might also have contributed to improvement in electrochemical performance of the prepared composites through providing the pathway of lower activation energy. For comparison, all the electrodes were run in the PBS (pH 8.0) without the drugs and showed improved background current in the order Ni-CoS/GCE < GQDs/GCE < Ni-CoS/GQDs/GCE, indicating no electroactive substances on the electrode surface and successful modification (Figure 6(a)). Hence, Ni-CoS/GQDs/GCE was used for the determination of LAM and TDF simultaneously with no overlap as shown by ΔE_{pa} of 400 mV on CV Figure 6.

3.5. Kinetic Studies. One major factor affecting electrooxidation of compounds is scan rate [27]. To prove its effects, a scan rate (v) from 30 to 160 mV s^{-1} on i_{pa} and E_{pa} for a

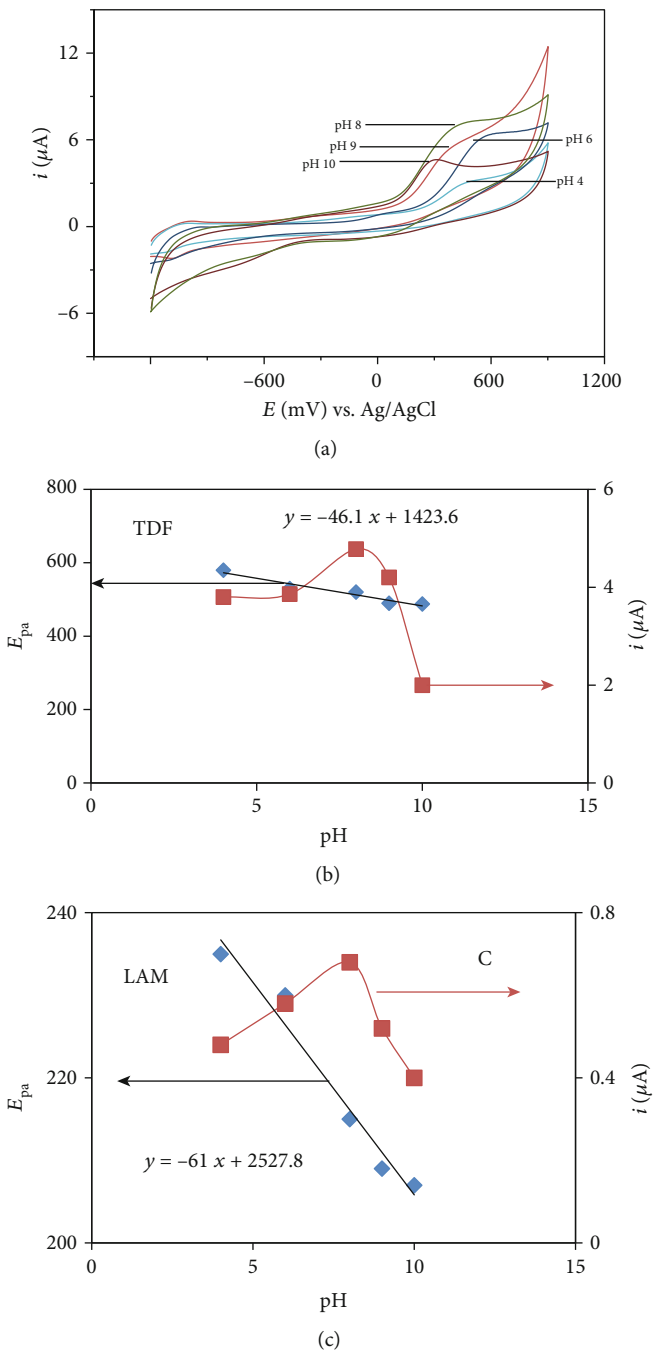

FIGURE 5: CVs (a): plot of i_{pa} and E_{pa} *vs.* pH for 1 mM TDF (b) and 1 mM LAM (c) in 0.1 M PBS at Ni-CoS/GQDs/GCE.

mixture of LAM and TDF in 0.1 M PBS (pH 8.0) was investigated (Figure 7). It can be seen that both compounds show i_{pa} increasing and E_{pa} shifting in the positive direction as the scan rate is increased. The increase in i_{pa} provides clear electrochemical reaction abilities and fast electron transfer kinetics of Ni-CoS at the Ni-CoS/GQDs/GCE. Furthermore, it might be due to favorable dispersion of Ni-CoS in GQDs coupled with excellent conductivity of the composite. The positive shift in E_{pa} observed with an increase in scan rate confirms irreversible oxidation nature of the process for both drugs. In Figure 7(a), dotted circle indicates increasing oxidative current for LAM. From Figure 7(b), i_{pa} increases linearly with scan rate (ν) for both compounds showing adsorption-related processes. To further verify this, plots of log i_{pa} against log ν (Figure 7(c)) gave slopes of LAM (0.55) and TDF (0.70). It can be deduced that both TDF and LAM showed mixed behavior since their slopes were greater than 0.5 [42]. Hence, adsorption and diffusion could have occurred during the simultaneous electrochemical process.

In order to find electron numbers in oxidation processes of TDF and LAM on modified Ni-CoS/GQDs/GCE, the Laviron equation for the irreversible electrode process was used [43]:

$$E_{pa}E^0 + \left(\frac{RT}{\alpha nF}\right) \ln\left(\frac{RTk^0}{\alpha nF}\right) + \left(\frac{RT}{\alpha nF}\right) \ln \nu, \quad (1)$$

where α is transfer coefficient, k^0 is the standard rate constant of the reaction, n is the electron transfer number involved in rate-determining step, ν is the scan rate, E^0 is the formal redox potential, R is the gas constant, T is the absolute temperature, and F is the Faraday constant. According to the slopes of the plot of E_{pa} versus ln ν, the αn values were calculated to be 0.92 (TDF) and (0.88) LAM. Generally, α is assumed to be 0.5 in a totally irreversible electrode process [40]. Therefore, the n values were found $1.84 \approx 2$ (TDF) and $1.76 \approx 2$ (LAM). The pH effect on E_{pa} demonstrated that the number of electrons and protons involved in both TDF and LAM oxidation is equal. Based on two electrons and two protons obtained, a possible oxidation mechanism for TDF on Ni-CoS/GQDs/GCE was given in Scheme 1(a) [44]. In this case, the adenine moiety in the TDF molecule is oxidized to give 2-oxoadenine product. No detailed electrochemical oxidation mechanism of LAM has been studied in the literature. Based on our experimental observation of the involvement of two electrons, we proposed a possible mechanism for LAM (Scheme 1(b)). In the present investigation, only a single oxidation peak for LAM is obtained in the pH range 4–10, which indicates the formation of mononitroso derivative by a two-electron process.

3.6. Effect of Different Drug Concentrations. Linear sweep voltammetry (LSV) was used to demonstrate adsorption behavior on Ni-CoS/GQDs/GCE. The effect of increasing concentrations of LAM or TDF in 0.1 M PBS on i_{pa} is shown (Figure 8). The association constant (K) of LAM or TDF with Ni-CoS/GQDs/GCE was deduced using equation (2) [45].

$$\frac{[\text{LAM or TDF}]}{i_{pa}} = \frac{i}{Ki_{max}} + \frac{[\text{LAM or TDF}]}{i_{max}}, \quad (2)$$

where i_{pa} is the anodic peak current for a given concentration of LAM or TDF, i_{max} is the maximum peak current, and K is the Langmuir adsorption constant of LAM or TDF with Ni-CoS/GQDs/GCE. To show absorptivity, applying the Langmuir theory involves a plotting ratio of LAM or TDF concentration to catalytic current against the concentration of LAM

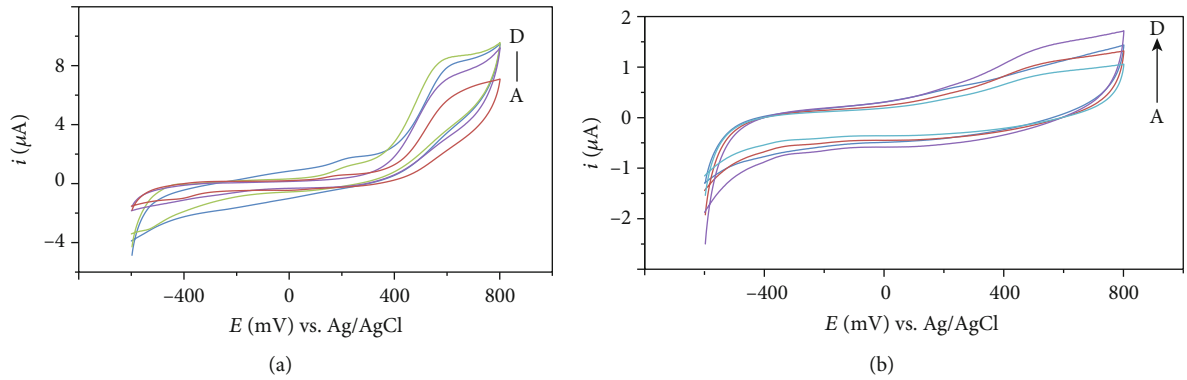

Figure 6: (a) CVs obtained at GCE (A), Ni-CoS/GCE (B), GQDs/GCE (C), and Ni-CoS/GQDs/GCE (D) electrodes in 0.1 M PBS (pH 8.0) with 1 mM LAM and TDF solution at a scan rate of 100 m V/s; (b) Ni-CoS/GQDs/GCE alone at a scan rate of 100 mV/s.

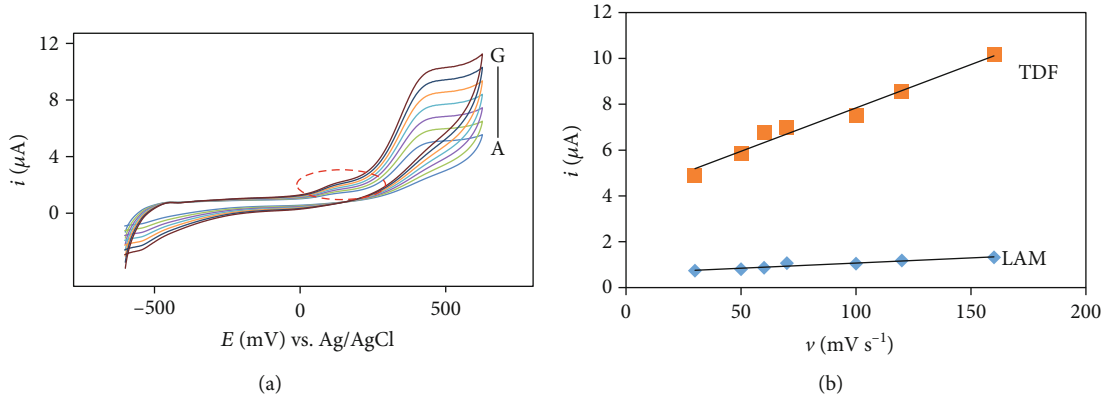

Figure 7: CVs of Ni-CoS/GQDs/GCE in 0.1 M PBS (pH 8.0) with 1 mM LAM and TDF solution at a different scan rate; (A–G) correspond to 30, 50, 60, 70, 100, 120, and 160 mV s^{-1}. (a) enlarged region of LAM oxidation at different scan rates; (b) i_{pa} (μA) vs. v (mV s^{-1}). (c) log i_{pa} (μA) vs. log v (mV s^{-1}).

or TDF and should show linearity. From the slopes and the intercepts of Figure 8, K was established as 9.0×10^{-2} M^{-1} (LAM) or 4.6×10^{-2} M^{-1} (TDF). It can also be concluded that the electrochemical response comes from the surface-confined LAM or TDF molecules adsorbed on Ni-CoS/GQDs/GCE after diffusion from the electrolyte solution. In addition, the Gibbs free energy changes (ΔG°) for adsorptive phenomenon form equation (3) were -54.6 kJ (LAM) and -69.8 kJ (TDF) showing that process was a spontaneous and favorable process [39].

$$\Delta G^{\bigcirc} = -RT \ln K, \tag{3}$$

where R is the molar gas constant and T is the room temperature.

Cyclic voltammetry detection of LAM or TDF was investigated from 10 to 50 μM at the modified electrode (Figure 9). As shown in Figure 9, with each successive addition of LAM or TDF, i_{pa} increased with a slight negative shift in E_{pa} indicating Ni-CoS/GQD composite acted as a possible catalyst towards simultaneous oxidation of drugs. A plot of i_{pa} *vs.* [LAM or TDF] gave a linear relationship (Figure 9(a)). In addition, the linear relationships from plots of log i_{pa} vs. log [LAM or TDF] (Figure 9(b)) imply first-order kinetics with respect to each of the analyte, giving the following rate equation:

$$r = k[\text{LAM}][\text{TDF}]. \tag{4}$$

3.7. Chronoamperometry Studies. Based on the voltammetric results, Ni-CoS/GQDs/GCE can effectively catalyze the oxidation of TDF and LAM, and it appears that chronoamperometry detection of the drugs by developed electrode is possible in order to determine rate constants. The rate constant can be evaluated using equation (5):

$$\frac{I_{cat}}{I_{buf}} = \frac{\gamma^{1/2}\left(\pi^{1/2}\,\text{erf}\left(\gamma^{1/2}\right) + \exp^{-\gamma}\right)}{\gamma^{1/2}}, \tag{5}$$

where I_{cat} and I_{buf} are currents on Ni-CoS/GQDs/GCE in the presence and absence of LAM or TDF, respectively, $\gamma = kC_o t$ (C_o is the bulk concentration of LAM or TDF), and erf is the error function. The error function is almost equal to 1 when γ exceeds to 2, and hence, equation (5) reduces to equation (6).

$$\frac{I_{cat}}{I_{buf}} = \gamma^{1/2}\pi^{1/2} = \pi^{1/2}(kC_o t)^{1/2}, \tag{6}$$

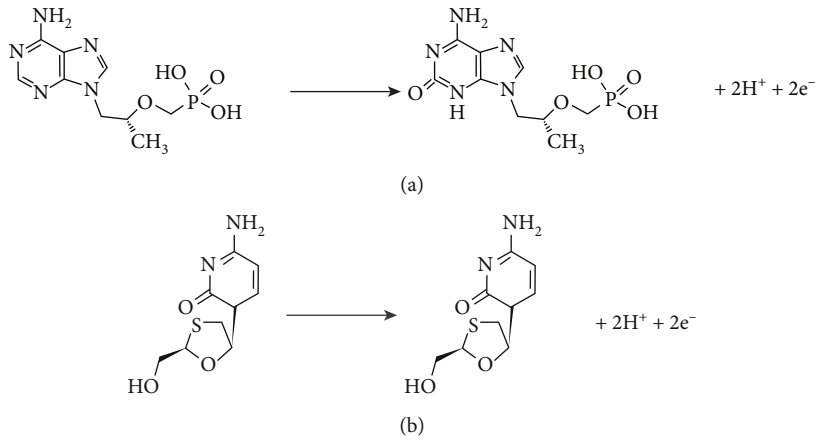

Scheme 1

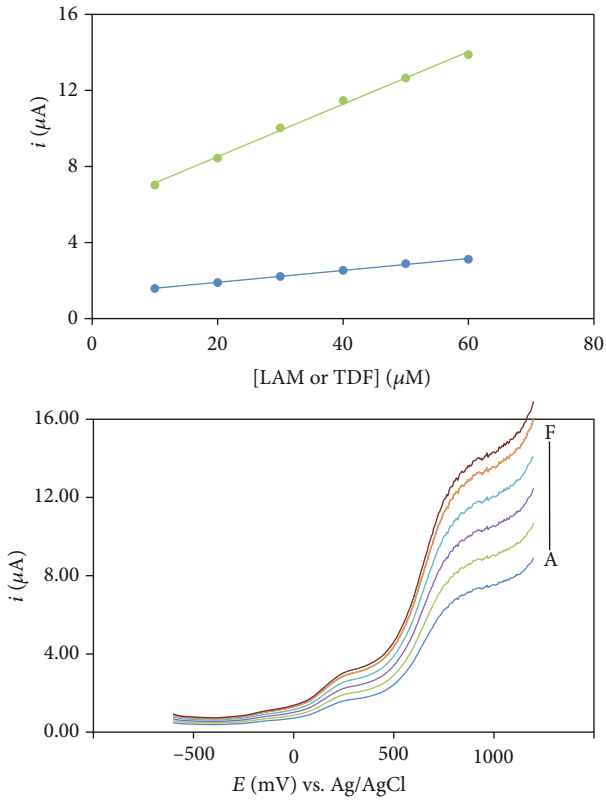

Figure 8: LSVs for different concentrations of TDF and LAM (A–F): 10, 20, 30, 40, 50, and 60 μM in 0.1 M PBS and Langmuir adsorption isotherm plot: i_{pa} employed.

where k is the catalytic rate constant and t is time elapsed in seconds. The catalytic rate constants for TDF and LAM were calculated based on information obtained from chronoamperometry (Figures 10(a) and 10(b)). The ratio of catalytic currents (I_{cat}) and buffer currents (I_{buffer}) versus time ($t^{1/2}$) during the rapid decay time gave linear plots. The square of the slopes against the respective concentrations (Figures 10(a) and 10(b), A and B) gave linear plots whose slope is equal to πk. The calculated values of catalytic constants were $5.80 \times 10^3\ M^{-1}\ s^{-1}$ (TDF) and $8.23 \times 10^3\ M^{-1}\ s^{-1}$ (LAM). The calculated values further elucidate sharp characteristics of the catalytic peak currents for oxidation of LAM and TDF.

3.8. DPV Analysis. Simultaneous determination of equal concentrations of LAM and TDF was investigated (Figure 11(a)). As shown in Figure 11(a), clearly well-resolved peaks can be seen, with ΔE_p potential of 620 mV for the addition of increasing concentrations. The plot of i_{pa} *vs.* [LAM] or [TDF] increased linearly with correlation coefficients of 0.998 and 0.997, respectively (Figure 11(a), A and B). The limit of detection (LOD) of both drugs were calculated as 3.3 times standard deviation for average measurements of blank samples (LOD = 3.3 × RSD/slope) [44]. The LODs (2.42×10^{-8} mM LAM; 1.21×10^{-8} mM TDF) and linear working range (LWR) (5-18 μM) were obtained. Our results compared well with those from literature for single determinations (Table 1) showing that Ni-CoS/GQDs/GCE provided a novel platform for the simultaneous detection. Consequently, it was concluded that using the proposed DPV method, the simultaneous determination of the two drugs was possible.

In sensors, reproducibility and storage stability are significant processes to be investigated. For reproducibility, the sensor was performed through five repetitive measurements of 0.18 μM of LAM and TDF simultaneously by DPV (Figure 11(b)). The relative standard deviation of i_{pa} responses to LAM, and TDF sensing was less than 4.6% indicating good reproducibility. For storage stability of sensor, current responses to 0.1 mM LAM and TDF were recorded each day. As shown in Figure 11(c), current responses at Ni-CoS/GQDs/GCE decreased to about 96% when compared to initial i_{pa} on the 8th day, representing long-term stability. The 4% loss in i_{pa} might be due to leaching of Ni-CoS/GQDs from the surface of the electrode. The adsorption of end products of oxidation blocking the catalytic sites of Ni-CoS/GQDs/GCE with TDF and LAM cannot be ruled out as another possible factor causing i_{pa} decrease in simultaneous oxidation.

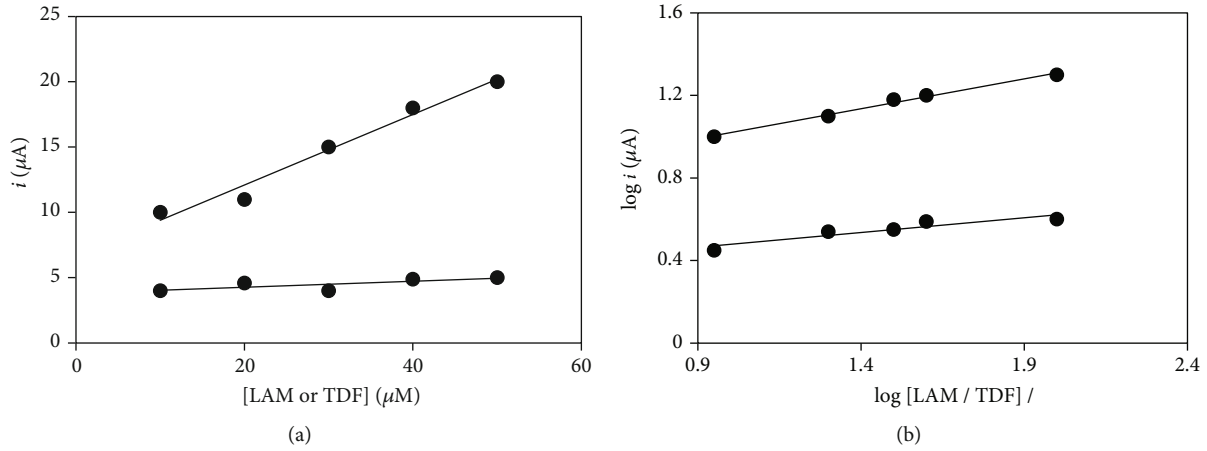

FIGURE 9: CVs obtained for drugs in the concentrations ranging from 10 to 50 μM (c, A–E), when LAM or TDF was added in steps of 10 μM each in 0.1 M PBS (pH 8). (a) shows calibration plots and (b) shows plot of log i_{pa} vs. log [LAM or TDF].

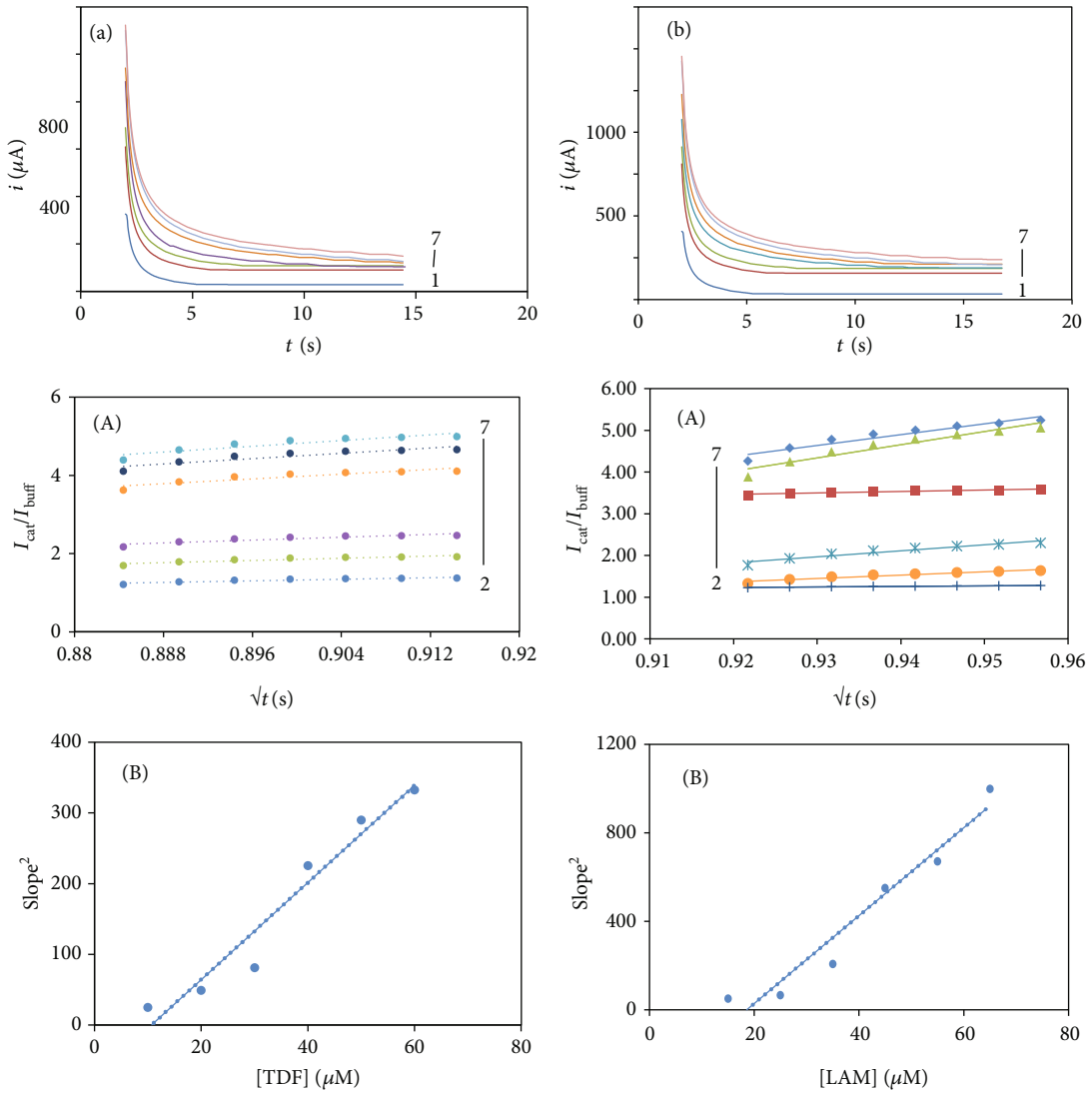

FIGURE 10: Chronoamperometry of (a) TDF (b) LAM in 0.1 M PBS (pH 8) (*curve 1*), (*curves 2-7*); 10-60 μM; (A) plots of I_{cat}/I_{buff} vs. $t^{1/2}$; (B) plot of slopes^2 against [TDF or LAM].

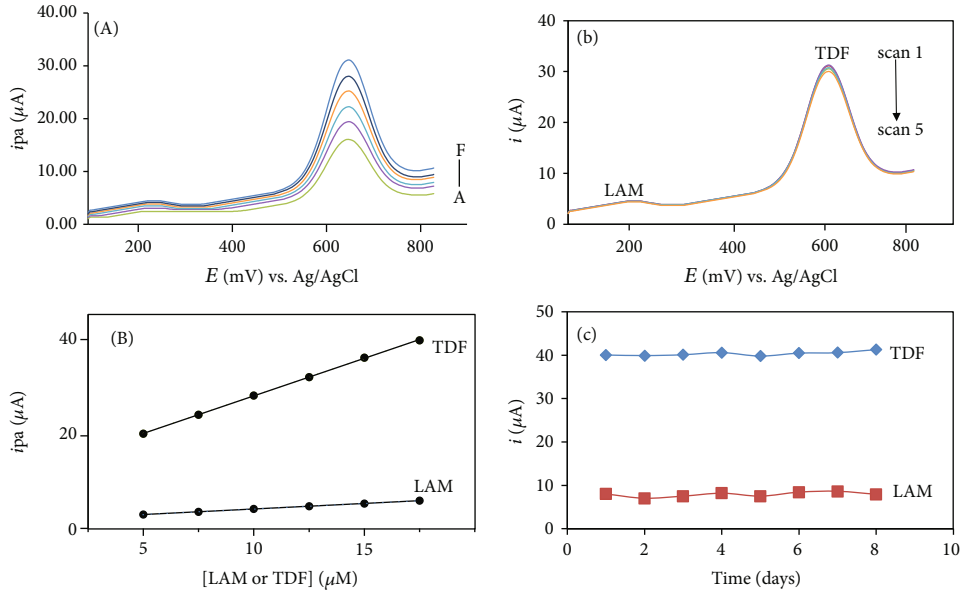

Figure 11: (a) DPV as a function of different LAM or TDF concentrations (a′) 5 μM, (b′) 8 μM, (c′) 10 μM, (d′) 12 μM, (e′) 15 μM, and (f′) 18 μM, (A, B) corresponding calibration plot of i_{pa} vs. [LAM or TDF]. (b) Reproducibility of the composite electrode after 5 runs in 0.1 M pH 8 PBS containing 12 μM of LAM and TDF. (c) Stability tests for a period of 8 days.

Table 1: Comparison of different chemically modified electrodes for the determination TDF and LAM.

Modifier	Technique	Type of buffer and pH	Type of determination	E_{pa} (mV)	LOD/mM	Reference
GCE	AdSDPV, AdSSWV	Acetate buffer solution; 4.7	Single	TDF (+1330)	1.02×10^{-7} M 8.40×10^{-8} M	[15]
BDDE	SWV	BR buffer; 4.0	Single	+1500	5.6×10^{-7}	[39]
NiCoS/GQDs/GCE	DPV	PBS; 8.0	Simultaneous	TDF (+598); LAM (+223)	TDF (1.21×10^{-8}); LAM (2.42×10^{-8})	Present work

Key: differential pulse voltammetry: DPV, square-wave voltammetry; SWV, adsorptive stripping differential pulse; AdSDPV: adsorptive stripping square wave voltammetry; AdSSWV; BDDE: boron-doped diamond electrode.

3.9. Impedimetric Sensing. EIS has mainly been used for electrode characterization using hexacyanoferrate as a redox probe and its use in analyte detection such as drugs which have not been reported frequently [13]. Impedimetric sensing of drugs has been done preliminarily in our research group and showed promising results [46]. In the present study, impedimetric sensing properties of Ni-CoS/GQDs/GCE with and without addition of TDF as an example was investigated. From Figure 12, a small R_{et} value (500 Ω) was observed after addition of the drug whilst R_{et} without addition of TDF was 1200 Ω, showing Ni-CoS/GQD composite responded well towards oxidation of TDF.

Oxidation reactions can generate electrons which can enhance electron transfer rates, decreasing R_{et} values hence allowing increased sensitivity of a sensor. In the present study, when TDF concentrations (Figure 13) were increased, R_{et} values decreased markedly, showing enhanced electrode transfer kinetics. The R_{et} is inversely proportional to logarithm of TDF concentrations with a linearity display (Figure 13) ($R^2 = 0.999$). The obtained results clearly reveal possibility of impedimetric detection of TDF using Ni-CoS/GQD composite. From these preliminary studies, quantification of some drugs by EIS is possible.

3.10. Selectivity. For demonstrating selectivity of Ni-CoS/GQDs/GCE, the EIS method was used. The fabricated sensor was incubated in the presence of some metal ions (Na^+, K^+) and possible biological molecules (glucose, dopamine, and uric acid) to a solution containing either LAM or TDF (0.2 mM) in the ratio of 1 : 10. R_{et} values (TDF; 0.5 kΩ), (LAM; 0.65 kΩ) were obtained before interactions. The effective ΔR_{et} by NaCl (+0.02 kΩ; +0.01 kΩ), KCl (+0.04 kΩ; +0.02 kΩ), glucose (-0.02 kΩ; -0.01 kΩ), dopamine (+0.01 kΩ; +0.02 kΩ), and uric acid (+0.05 kΩ; +0.02 kΩ) were calculated for TDF and LAM, respectively. By looking at all obtained small values, it can be concluded that the sensor had good selectivity and good anti-interference ability based on the combination of Ni-CoS

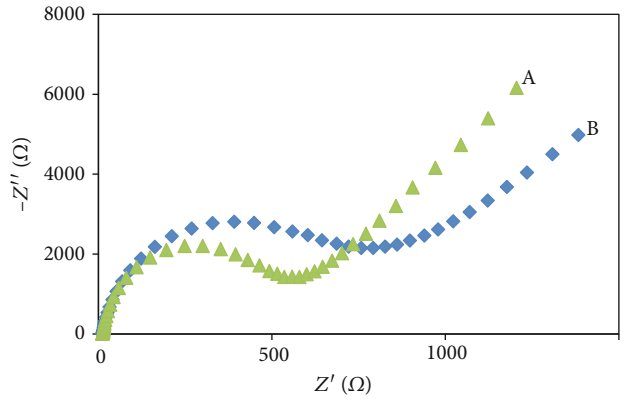

Figure 12: Impedimetric response of Ni-CoS/GQDs/GCE (a) with TDF (1 mM) (b) without TDF.

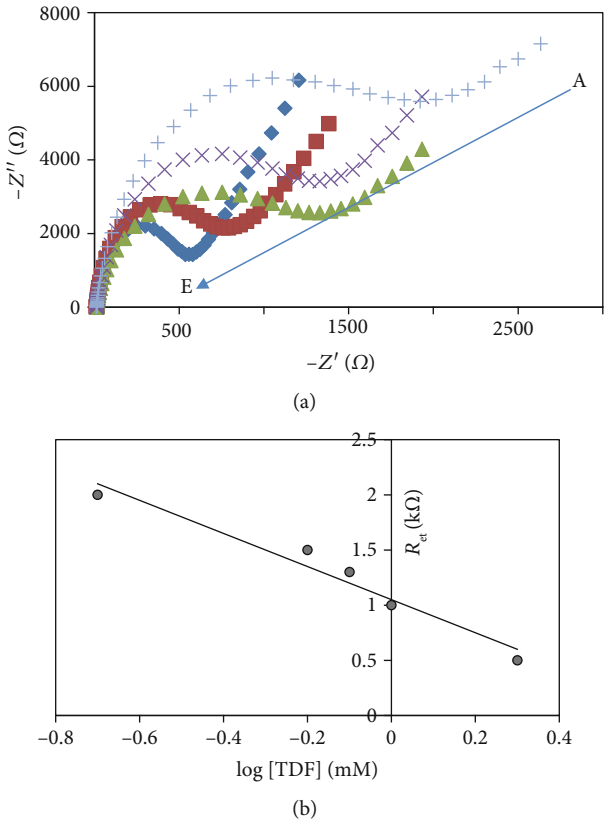

Figure 13: (a) EIS spectra at Ni-CoS/GQDs/GCE for different TDF concentrations (A–E; 0.2nnn- 1 mM): in PBS (pH 8.0). (b) Variation of R_{et} with log [TDF]/mM.

and GQD properties discussed before. Values for ΔR_{et} were obtained as R_{et} $(_{\text{after interaction}})$ − R_{et} $(_{\text{before interaction}})$.

3.11. Analysis of Real Samples

3.11.1. Determination of TDF and LAM in Formulation Tablets. The fabricated electrode was successfully applied for direct determination of LAM and TDF in a pharmaceutical formulation containing 300 mg/tablet and 450 mg/tablet, respectively (Table 2).

Table 2: Results of the assay from TDF, LAM, and the recovery assay.

	TDF	LAM
Pharmaceutical formulation		
Labeled claim (mg)	450	300
Amount found (mg)∗	450.02	301.30
RSD%	1.13	1.67
Pure TDF, LAM added to tablet solution		
Added (mg)	15.0	15.0
Found (mg)∗	14.7	15.2
Recovery (%)	98 ± 0.01	101.3
RSD%	1.2	1.3

∗Each value is the mean of five experiments.

Table 3: Determination of the drugs in urine.

	LAM			TDF	
Added (μM)	Found (μM)	Recovery (%)	Added (μM)	Found (μM)	Recovery (%)
20	21.05	105 ± 0.02	20	19.40	97 ± 0.02
25	26.10	104 ± 0.01	25	23.98	96 ± 0.03
30	31.50	105 ± 0.01	30	30.30	101 ± 0.02
35	37.01	106 ± 0.02	35	34.31	98 ± 0.01

TDF and LAM in aqueous samples were too low for detection using the sensor; hence, spiking with different concentrations was demonstrated. The recovery was obtained by using DPV to evaluate the accuracy of the method. The relative standard deviation of this method, based on five replicates ($n = 5$), is presented in Table 2. It can be reported that satisfactory recoveries of TDF and LAM at Ni-CoS/GQDs/GCE in the range of 98–101.3% revealed that the proposed method is effective and reliable. The findings indicated that the method is rapid and simple for the selective and sensitive analysis of TDF and LAM in pharmaceutical preparations.

3.11.2. Determination of TDF and LAM in Urine Samples. The Ni-CoS/GQDs/GCE was investigated for the measurement of TDF and LAM in four human urine samples. The percentage of recovery of the spiked sample is in the range between 96.0 and 106 (Table 3). The results show that the modified electrode is suitable for the determination of TDF and LAM in biological fluids.

4. Conclusion

For the first time, simultaneous electrochemical behavior of TDF and LAM was examined. It was also illustrated that Ni-CoS/GQDs/GCE offered a stable low potential during drug detection. The negative values of change in Gibbs free energy revealed that adsorption of both drugs on the modified electrode is spontaneous. The obtained Ni-CoS/GQD composite exhibited good reproducibility and stability

during analysis. The present study provides a general strategy for using different transitional elements for decorating graphene quantum dots for different applications.

Data Availability

The data used to support the findings of this study are included within the article.

Conflicts of Interest

The authors declare no conflicts of interest and the mentioned received funding did not lead to any conflicts of interest regarding the publication of this manuscript.

Authors' Contributions

Ruvimbo Chihava, Daniel Apath, and Mambo Moyo conceived and designed the experiments and wrote the paper; Munyaradzi Shumba performed and construed chronoamperometric experiments; Vitalis Chitsa and Piwai Tshuma analyzed the data.

Acknowledgments

The authors would like to acknowledge Midlands State Research Board for funding.

Supplementary Materials

Figure 1S: CVs obtained in 2 mM $[Fe(CN)6]^{3-/4-}$ in 1 M KCI; (a) GCE (b) Ni-CoS/GCE, (c) GQDs/GCE, and (d) Ni-CoS/GQDs/GCE. *(Supplementary Materials)*

References

[1] N. L. Teradal, S. N. Prashanth, and J. Seetharamappa, "Electrochemical studies of nevirapine, an anti-HIV drug, and its assay in tablets and biological samples," *Journal of Electrochemical Science and Engineering*, vol. 2, no. 2, pp. 67–75, 2012.

[2] B. Bozal, B. Uslu, and S. A. Ozkan, "A review of electroanalytical techniques for determination of anti-HIV drugs," *International Journal of Electrochemistry*, vol. 2011, 17 pages, 2011.

[3] P. B. Kandagal, D. H. Manjunatha, J. Seetharamappa, and S. S. Kalanur, "RP-HPLC method for the determination of tenofovir in pharmaceutical formulations and spiked human plasma," *Analytical Letters*, vol. 41, no. 4, pp. 561–570, 2008.

[4] D. A. Kumar, G. S. Rao, and J. V. L. N. S. Rao, "Simultaneous determination of lamivudine, zidovudine and abacavir in tablet dosage forms by RP HPLC method," *E-Journal of Chemistry*, vol. 7, no. 1, pp. 180–184, 2010.

[5] S. Notari, M. Sergi, C. Montesano et al., "Simultaneous determination of lamivudine, lopinavir, ritonavir, and zidovudine concentration in plasma of HIV-infected patients by HPLC-MS/MS," *IUBMB Life*, vol. 64, no. 5, pp. 443–449, 2012.

[6] A. B. Babu, G. Ramu, C. M. Krishna, and S. B. Reddy, "Spectrophotometric determination of lamivudine in pure and tablet forms," *E-Journal of Chemistry*, vol. 9, no. 2, pp. 569–575, 2012.

[7] M. Himaja, J. Kalpana, and C. Anbarasu, "Validated zero order and first order derivative spectrophotometric methods for invitro analysis of tenofovir disoproxil fumarate tablets using azeotropic mixture," *International Journal of Pharmaceutical Science*, vol. 6, no. 6, pp. 302–304, 2014.

[8] R. Sharma and K. Mehta, "Simultaneous spectrophotometric estimation of tenofovir disoproxil fumarate and lamivudine in three component tablet formulation containing efavirenz," *Indian Journal of Pharmaceutical Science*, vol. 72, no. 4, pp. 527–530, 2010.

[9] B. Uslu and S. A. Özkan, "Determination of lamivudine and zidovudine in binary mixtures using first derivative spectrophotometric, first derivative of the ratio-spectra and high-performance liquid chromatography-UV methods," *Analytica Chimica Acta*, vol. 466, no. 1, pp. 175–185, 2002.

[10] N. Kapoor, S. Khandavilli, and R. Panchagnula, "Simultaneous determination of lamivudine and stavudine in antiretroviral fixed dose combinations by first derivative spectrophotometry and high performance liquid chromatography," *Journal Pharmaceutical Biomedical Analysis*, vol. 41, no. 3, pp. 761–765, 2006.

[11] G. Sankar, M. V. Reddy, J. M. R. Kumar, and T. K. Murthy, "Spectrophotometric determination of lamivudine and stavudine," *Indian Journal Pharmaceutical Sciences*, vol. 64, no. 5, pp. 504–506, 2002.

[12] N. Aliakbarinodehi, P. Jolly, N. Bhalla et al., "Aptamer-based field-effect biosensor for tenofovir detection," *Scientific Reports*, vol. 7, article 44409, 2017.

[13] T. Bhengo, M. Moyo, M. Shumba, and J. Okonkwo, "Simultaneous oxidative determination of antibacterial drugs in aqueous solutions using an electrode modified with MWCNTs decorated with Fe_3O_4 nanoparticles," *New Journal of Chemistry*, vol. 42, no. 7, pp. 5014–5023, 2018.

[14] R. Jain and R. Sharma, "Cathodic adsorptive stripping voltammetric detection and quantification of the antiretroviral drug tenofovir in human plasma and a tablet formulation," *Journal of Electrochemical Society*, vol. 160, pp. 489–493, 2013.

[15] G. Ozcelikay, B. Dogan-Topal, and S. A. Ozkan, "Electrochemical characteristics of tenofovir and its determination in dosage form by electroanalytical methods," *Revue Roumaine de Chimie*, vol. 62, no. 6-7, pp. 569–578, 2017.

[16] B. Dogan, B. Uslu, S. Suzen, and S. A. Ozkan, "Electrochemical evaluation of nucleoside analogue lamivudine in pharmaceutical dosage forms and human serum," *Electroanalysis*, vol. 17, no. 20, pp. 886–1894, 2005.

[17] R. Jain, N. Jadon, and K. Radhapyari, "Cathodic adsorptive stripping voltammetric studies on lamivudine: an antiretroviral drug," *Journal of Colloid Interface Science*, vol. 313, no. 1, pp. 254–260, 2007.

[18] K. C. Leandro, J. C. Moreira, and P. A. M. Farias, "Differential pulse voltammetric studies on lamivudine: an antiretroviral drug," *American Journal of Analytical Chemistry*, vol. 4, no. 6, pp. 47–51, 2013.

[19] N. Ding, N. Yan, C. Ren, and X. Chen, "Colorimetric determination of melamine in dairy products by Fe_3O_4 magnetic nanoparticles–H_2O_2–ABTS detection system," *Analytical Chemistry*, vol. 82, no. 13, pp. 5897–5899, 2010.

[20] J. Bai and X. Jiang, "A facile one-pot synthesis of copper sulfide- decorated reduced graphene oxide composites for enhanced detecting of H_2O_2 in biological environments," *Analytical Chemistry*, vol. 85, no. 17, pp. 8095–8101, 2013.

[21] X. Cai, X. Shen, L. Ma, Z. Ji, and L. Kong, "Facile synthesis of nickel-cobalt sulfide/reduced graphene oxide hybrid with

enhanced capacitive performance," *Journal of the Royal Society of Chemistry Advances*, vol. 5, no. 72, pp. 58777–58783, 2015.

[22] J. Zou, J. Jiang, L. Huang, H. Jiang, and K. Huang, "Synthesis, characterization and electrocatalytic activity of copper sulfide nanocrystals with different morphologies," *Journal of Solid State Sciences*, vol. 13, no. 6, pp. 1261–1267, 2011.

[23] F. Zhao, W. Huang, and D. Zhou, "Chemical bath deposition synthesis of nickel cobalt oxides/sulfides for high-performance supercapacitors electrode materials," *Journal of Alloys Compound*, vol. 75, pp. 15–23, 2018.

[24] G. He, Y. Song, K. Liu, A. Walter, S. Chen, and S. Chen, "Oxygen reduction catalyzed by platinum nanoparticles supported on graphene quantum dots," *ACS Catalysis*, vol. 3, no. 5, pp. 831–838, 2013.

[25] W. W. Liu, Y. Q. Feng, X. B. Yan, J. T. Chen, and Q. J. Xue, "Superior micro-supercapacitors based on graphene quantum dots," *Advanced Functional Materials*, vol. 23, no. 33, pp. 4111–4122, 2013.

[26] J. Zhao, G. Chen, L. Zhu, and G. Li, "Graphene quantum dots-based platform for the fabrication of electrochemical biosensors," *Journal of Electrochemistry Communications*, vol. 13, no. 1, pp. 31–33, 2011.

[27] N. Hashemzadeh, M. Hasanzadeh, N. Shadjou, J. Eivazi-Ziaei, M. Khoubnasabjafari, and A. Jouyban, "Graphene quantum dot modified glassy carbon electrode for the determination of doxorubicin hydrochloride in human plasma," *Journal of Pharmaceutical Analysis*, vol. 6, no. 4, pp. 235–241, 2016.

[28] V. Usai, T. Mugadza, F. Chigondo et al., "Synthesis and characterisation of cobalt oxide nanoparticles decorated graphene oxide and its electrocatalytic behaviour," *Polyhedron*, vol. 157, pp. 192–199, 2019.

[29] S. Gupta, T. Smith, A. Banaszak, and J. Boeckl, "Graphene quantum dots electrochemistry and sensitive electrocatalytic glucose sensor development," *Journal of Nanomaterials*, vol. 7, no. 10, 2017.

[30] Z. Chen, Z. Wan, T. Yang et al., "Preparation of nickel cobalt sulfide hollow nanocolloids with enhanced electrochemical property for supercapacitors application," *Scientific Reports*, vol. 6, article 25151, 2016.

[31] D. Y. Kim, G. S. Ghodake, N. C. Maile, A. A. Kadam, D. S. Lee, and S. K. Shinde, "Chemical synthesis of hierarchical $NiCo_2S_4$ nanosheets like nanostructure on flexible foil for a high performance supercapacitor," *Scientific Reports*, vol. 7, no. 1, article 9764, 2017.

[32] M. K. Sahoo and G. R. Rao, "Fabrication of $NiCo_2S_4$ nanoball embedded nitrogen doped mesoporous carbon on nickel foam as an advanced charge storage material," *Journal of Electrochemica Acta*, vol. 268, pp. 139–149, 2018.

[33] Z. Ciplak, N. Yildiz, and A. Calimli, "Investigation of graphene/Ag nanocomposites synthesis parameters for two different synthesis methods," *Fullerenes, Nanotubes, and Carbon Nanostructures*, vol. 23, no. 4, pp. 361–370, 2014.

[34] E. Zor, E. Morales-Narváez, A. Zamora-Gálvez, H. Bingol, M. Ersoz, and A. Merkoç, "Graphene quantum dots-based photoluminescent sensor: a multifunctional composite for pesticide detection," *Journal of American Society, ACS Applied Material. Interfaces*, vol. 7, no. 36, pp. 20272–20279, 2015.

[35] L. M. Dong, D. Y. Shi, Z. Wu, Q. Li, and Z. D. Han, "Improved solvothermal method for cutting graphene oxide into graphene quantum dots," *Digest Journal of Nanomaterials and Biostructures*, vol. 10, no. 3, pp. 855–864, 2015.

[36] F. Chekin, S. Bagheri, and ,S. B. A. Hamid, "Synthesis of graphene oxide nanosheet: a novel glucose sensor based on nickel–graphene oxide composite film," *Russian Journal of Electrochemistry*, vol. 50, no. 11, pp. 1044–1049, 2014.

[37] Y. Zhang, M. Ma, J. Yang et al., "Shape-controlled synthesis of $NiCo_2S_4$ and their charge storage characteristics in supercapacitors," *Nanoscale*, vol. 6, no. 16, pp. 9824–9830, 2014.

[38] M. Shumba and T. Nyokong, "Electrode modification using nanocomposites of boron or nitrogen doped graphene oxide and cobalt (II) tetra aminophenoxy phthalocyanine nanoparticles," *Electrochimica Acta*, vol. 196, pp. 457–469, 2016.

[39] K. Morawska, T. Popławski, W. Ciesielski, and S. Smarzewska, "Electrochemical and spectroscopic studies of the interaction of antiviral drug tenofovir with single and double stranded DNA," *Bioelectrochemistry*, vol. 123, pp. 227–232, 2018.

[40] A. J. Bard and L. R. Faulkner, *Electrochemical Methods: Fundamentals Applications*, Wiley, New York, 2nd edition, 1980.

[41] Y. Seekaew, O. Arayawut, K. Timsorn, and C. Wongchoosuk, "Synthesis, characterization, and applications of graphene and derivatives," in *Carbon-Based Nanofillers and their Rubber Nanocomposites*, pp. 259–283, Elsevier Inc, 2019, chapter 9.

[42] M. Moyo, R. F. Lehutso, and O. J. Okonkwo, "Improved electro-oxidation of triclosan at nano-zinc oxide-multiwalled carbon nanotube modified glassy carbon electrode," *Sensors and Actuators B*, vol. 209, pp. 898–905, 2015.

[43] E. Laviron, "Adsorption, autoinhibition and autocatalysis in polarography and in linear potential sweep voltammetry," *Journal of Electroanalytical Chemistry*, vol. 52, no. 3, pp. 355–393, 1974.

[44] G. Ozcelikay, B. Dogan-Topal, and S. A. Ozkan, "An electrochemical sensor based on silver nanoparticles-benzalkonium chloride for the voltammetric determination of antiviral drug tenofovir," *Electroanalysis*, vol. 30, pp. 1–13, 2018.

[45] M. Moyo, P. Mudarikwa, and M. Shumba, "Voltammetric sensing of nitrite in aqueous solution using titanium dioxide anchored multiwalled carbon nanotubes," *Ionics*, vol. 24, no. 8, pp. 2489–2498, 2018.

[46] R. Chihava, M. Moyo, and M. Shumba, "Impedimetric determination of antiretroviral drugs on a modified glassy carbon electrode," in *2018 IEEE SENSORS*, pp. 1–4, New Delhi, India, 2018.